PAPER • OPEN ACCESS

PID vs. Backstepping Control for Cooperative Quadrotors Unmanned Aerial Vehicles

View the article online for updates and enhancements.

PID vs. Backstepping Control for Cooperative Quadrotors Unmanned Aerial Vehicles

M. Mahfouz [1, 4], A. Taiomour [2, 5], Mahmoud M. Ashry [1, 6], G. Elnashar [3,7].

[1]Department of Optoelectronics and Control, [2]Aircraft Armament Department, Military Technical College, [3]Commandant of MTC, Cairo, Egypt

E-mail: [4]m.mahfouz.trc@gmail.com, [5]a.taimour @mtc.edu.eg, [6]maashry@mtc.edu.eg, and [7]g.elnshar @mtc.edu.eg.

Abstract. Formation reconfiguration is one of the m st important tactics used in the field of cooperative Unmanned Air Vehicles. In this paper, formation reconfiguration for a team of vertical takeoff and landing quadrotors is managed by a classical approach of proportional-integral-derivative (PID) controller. PID controller is designed to regulate the attitude and the altitude for every quadrotor of a cooperative team respecting the separating span and velocity constraints. PID controller results are compared with a backstepping controller developed for the same system. The mathematical model of the propositioned system is derived initially, and then a PID controller using simplex and genetic algorithms is designed qualifying the cooperative quadrotors to track the desired trajectories. Simulation results present the assessment of PID control strategy along with backstepping control strategy in different scenarios including proposal flight mission in obstacle-free surroundings, and obstacle-laden surroundings. Noise attenuation and disturbance rejection are examined for both controllers to check the robustness of the system.

Keywords: Q   otor, Unmanned Air Vehicles, PID, Backstepping.

1. Introduction

In the latest decennary, cooperative Unmanned Air Vehicles (UAVs) draws increasable interest with their prosperity in several tasks through the implementation of various remarkable applications in both civil and military domains [1-6]. UAVs are characterized by performing the desired missions without human interference [7, 8]. The vertical takeoff and landing (VTOL) quadrotor UAV opens the gate to accomplish unparalleled tasks due to its special characteristics. Small size, lightweight, high agility, maneuverability, its ability of hovering, and vertical takeoff and landing are some of its amazing criteria [9-12]. Quadrotor UAVs characteristics guarantee a safety work capability with zero risks to the pilot in D-cube atmosphere (dirty, dull, and dangerous atmosphere) [13]. Therefore, quadrotor is utilized in many potential exercises such as surveillance, monitoring, patrolling, surveying and mapping, inspection and assistance duties, exploration, carriage and transportation, delivery, archeological, investigation and police assessment, loading military instruments, research, and education [11, 12, 14-17].

The promising performance of a single UAV in several applications encourages the utilization of multiple UAVs cooperating along to meet the specified tasks [18]. Cooperative UAVs ensure the success of the desired missions with better performance compared with single UAV [19]. Multiple

cooperative quadrotor UAVs required certain strategies to cooperate together to achieve the required goal [20]. These strategies are defined as the manner the cooperative UAVs act together and are known with UAVs tactics. One of these tactics is formation reconfiguration. Formation reconfiguration is defined by the capability of numerous cooperative UAVs to preserve a desired geometric structure and reconfigure to another formation based on the enclosing circumstances guaranteeing the success of the required application [21]. Every cooperative UAV in the team should follow Reynold's rules of flocking through the whole tour of the flight [22]. Every UAV member has to identify its velocity and separating span with its neighbors and avoid colliding with its neighbors or obstacles [23-25].

In this paper, the issue of formation reconfiguration for a team of unmanned cooperative quadrotors is solved using a designed PID controller. The designed controller is developed to control every unmanned quadrotor in the team in a decentralized style saving the reserving of the desired geometric structure. The proposed controller should carry out output behavior similar to those of the real system [26, 27]. Unlike the conventional VTOL air vehicles; the quadrotors are distinguished by a simple structure and paradigm form [16]. However, the intricacy of regulating the quadrotors during autonomous flight has become a major challenge for engineering and researchers. This is due to its anonymous nonlinearities and coupled variables [15]. The proposed designed regulator has the capacity to manage the under-actuated attributes and the nonlinearities of the quadrotors. PID controller is utilized to handle the nonlinearities and multivariable coupling saving the stabilization of the entire control system.

The major contribution in this paper lies in resolving the formation problem for a team of unmanned cooperative quadrotors in a decentralized style with various control techniques. Every quadrotor has the capacity to retain the desired position robustly during the entire flight stages even in maneuver keeping the desired formation of the whole cooperative team. The designed decentralized controller guarantees the success of the required mission of the team even in case of members' failure. Eventually, various simulations will be represented to validate the success of the designed controller in different approaches. The results of each approach are discussed. The simulation results declare the stability of the system and guarantee the reserving of the desired geometric formation.

This paper is sectioned as upcoming:

Section 2 explains the mathematical model of the quadrotors. PID and backstepping controllers are clarified in section 3. Section 4 displays the synthesis and simulation results of trajectory tracking using both PID and backstepping controllers for a team of cooperative quadrotors. Finally, the conclusion is briefed in section 5.

2. Quadrotor UAV Mathematical Model

The quadrotor is a multifaceted UAV as it is resilient to accomplish various missions and complicated orders to complete its classified roles successfully [14]. The quadrotor is a small agile air vehicle controlled by the independent speed variation of every rotor the quadruple rotors [9, 11]. Every rotor is bitched mounted identically from the centric pivot. The whole rotors are set to generate the demanded forces to every type of quadrotor motions. The underlying controller is designed for the OS4 quadrotor UAV model [28, 29].

For a team of similar cooperative quadrotors, assume every quadrotor of the team is a single solid frame with a 6-degree-of-freedom (6-DOF) as shown in Figure 1.
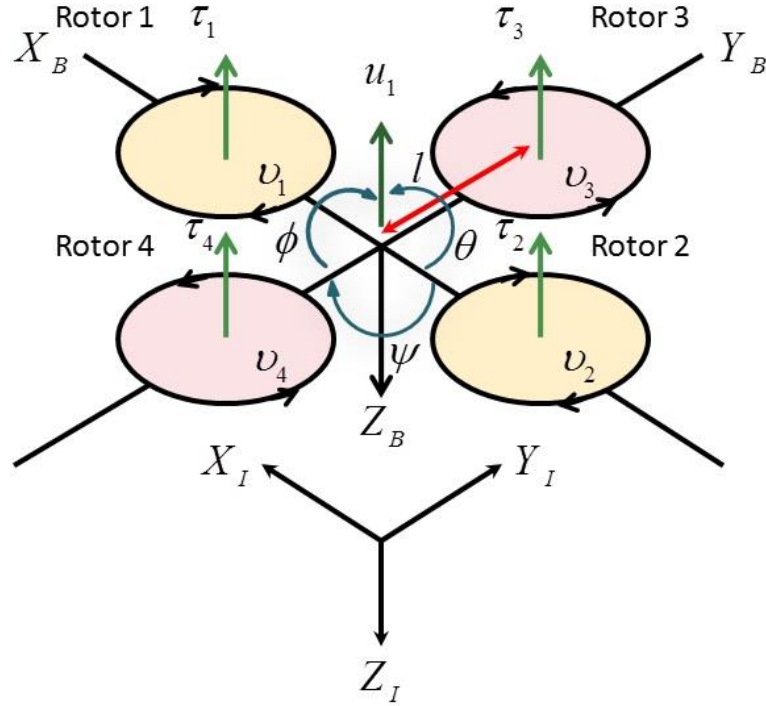
Figure 1. Quadrotor schematic platform.

2.1. *Mathematical Model*

Let τ_n and υ_n are the thrust and the torque respectively from the nth rotor and i^{th} quadrotor, the affected inputs can be summarized as follow [30]:

The whole thrust: $u_{1i} = \tau_{1i} + \tau_{2i} + \tau_{3i} + \tau_{4i}$ (1)

The roll moment: $u_{2i} = l_i (\tau_{3i} - \tau_{4i})$ (2)

The pitch moment: $u_{3i} = l_i (\tau_{1i} - \tau_{2i})$ (3)

The yaw moment: $u_{4i} = \upsilon_{1i} + \upsilon_{2i} - \upsilon_{3i} - \upsilon_{4i}$ (4)

For quadrotor as a flying platform; coordinates systems and reference frames must be considered in describing several dynamical coefficients and acting forces on the quadrotor. These forces have various reference frames. So, coordinates conversion between these frames is substantial. This conversion is achieved utilizing Euler's angles method [31, 32]. Suppose ϕ_i, θ_i, ψ_i represents the roll, pitch and yaw channels for i^{th} quadrotor respectively; the conversion from earth to body frame is illustrated in the direction cosine matrix R_{xyzi} as in (5) [33]:

$$R_{xyzi} = \begin{bmatrix} \sin\phi_i \sin\theta_i \sin\psi_i + \cos\theta_i \cos\psi & \sin\phi_i \sin\theta_i \cos\psi_i - \cos\theta_i \sin\psi_i & \cos\phi_i \sin\theta_i \\ \cos\phi_i \sin\psi_i & \cos\phi_i \cos\psi_i & -\sin\phi_i \\ \sin\phi_i \cos\theta_i \sin\psi_i - \sin\theta_i \cos\psi_i & \sin\phi_i \cos\theta_i \cos\psi_i + \sin\theta_i \sin\psi_i & \cos\phi_i \cos\theta_i \end{bmatrix} \quad (5)$$

Consider x_i, y_i, and z_i symbolize the frame posture for every agent of the cooperative quadrotors, so:

$$\ddot{x}_i = -\frac{\sin\theta_i \cos\phi_i}{m_i} u_{1i} \quad (6)$$

$$\ddot{y}_i = \frac{\sin\phi_i}{m_i} u_{1i} \quad (7)$$

$$\ddot{z}_i = -\frac{\cos\theta_i \cos\phi_i}{m_i} u_{1i} + g \tag{8}$$

Euler angular rates can be related to body angular rates as in (9):

$$\begin{bmatrix} \dot{\phi}_i \\ \dot{\theta}_i \\ \dot{\psi}_i \end{bmatrix} = \begin{bmatrix} \cos\psi_i & -\sin\psi_i & 0 \\ \frac{\sin\psi_i}{\cos\phi_i} & \frac{\cos\psi_i}{\cos\phi_i} & 0 \\ \sin\psi_i \tan\phi_i & \cos\psi_i \tan\phi_i & 1 \end{bmatrix} \begin{bmatrix} p_i \\ q_i \\ r_i \end{bmatrix} \tag{9}$$

Differentiating (9) will give:

$$\begin{bmatrix} \ddot{\phi}_i \\ \ddot{\theta}_i \\ \ddot{\psi}_i \end{bmatrix} = \begin{bmatrix} 0 & -\dot{\psi}_i \cos\phi_i & 0 \\ \frac{\dot{\psi}_i}{\cos\phi_i} & \dot{\phi}_i \tan\phi_i & 0 \\ \dot{\psi}_i \tan\phi_i & \frac{\dot{\phi}_i}{\cos\phi_i} & 0 \end{bmatrix} \begin{bmatrix} \dot{\phi}_i \\ \dot{\theta}_i \\ \dot{\psi}_i \end{bmatrix} + \begin{bmatrix} \cos\psi_i & -\sin\psi_i & 0 \\ \frac{\sin\psi_i}{\cos\phi_i} & \frac{\cos\psi_i}{\cos\phi_i} & 0 \\ \sin\psi_i \tan\phi_i & \cos\psi_i \tan\phi_i & 1 \end{bmatrix} \begin{bmatrix} \dot{p}_i \\ \dot{q}_i \\ \dot{r}_i \end{bmatrix} \tag{10}$$

The equality case of inertia along the *X*-orientation and *Y*-orientation yields:

$$\begin{cases} \ddot{\phi}_i = -\dot{\psi}_i \dot{\theta}_i \cos\phi_i + \frac{\cos\psi_i}{I_{xxi}} u_{2i} - \frac{\sin\psi_i}{I_{yyi}} u_{3i} + \frac{I_{yyi} - I_{zzi}}{I_{xxi}} (\dot{\psi}_i - \dot{\theta}_i \sin\phi_i)\dot{\theta}_i \cos\phi_i \\[2mm] \ddot{\theta}_i = \frac{\dot{\psi}_i \dot{\phi}_i}{\cos\phi_i} + \dot{\phi}_i \dot{\theta}_i \tan\phi_i + \frac{\sin\psi_i}{I_{xxi}\cos\phi_i} u_{2i} + \frac{\cos\psi_i}{I_{yyi}\cos\phi_i} u_{3i} - \frac{I_{yyi} - I_{zzi}}{I_{xxi}} (\dot{\psi}_i - \dot{\theta}_i \sin\phi_i)\frac{\dot{\phi}_i}{\cos\phi_i} \\[2mm] \ddot{\psi}_i = \dot{\psi}_i \dot{\phi}_i \tan\phi_i + \frac{\dot{\phi}_i \dot{\theta}_i}{\cos\phi_i} + \frac{\sin\psi_i \tan\phi_i}{I_{xxi}} u_{2i} + \frac{\cos\psi_i \tan\phi_i}{I_{yyi}} u_{3i} + \frac{1}{I_{zzi}} u_{4i} - \frac{I_{yyi} - I_{zzi}}{I_{xxi}} (\dot{\psi}_i - \dot{\theta}_i \sin\phi_i)\dot{\phi}_i \tan\phi_i \end{cases} \tag{11}$$

The relation between the thrust and the rotational speed for every rotor is investigated practically in [34], and the torque υ_n for n^{th} rotor and i^{th} quadrotor can be expressed mathematically as:

$$\upsilon_{ni} = \frac{\tau_{ni}(V_{Ci} + v_{ni}) + 0.125\rho_i b_i c_i R_{pi}^4 \omega_{m\_ni}^3 C_{di}}{\omega_{m\_ni}} \tag{12}$$

where, for i^{th} quadrotor; τ_{ni} is the thrust acting on the nth rotor; V_{Ci} is the vertical speed; v_{ni} is the induced velocity; ρ_i is the air density; b_i is the number of blades; c_i is the chord of the blade; R_{pi} is the radius of the propeller; ω_{m_ni} is the motor angular speed ; and C_{di} is the drag coefficient.

Newton-Euler formalism is utilized in expressing the quadrotors frame under external forces exercised to the centric pivot as [35]:

$$F_i^b = m_i \dot{v}_i^b + \omega_i^b \times m_i v_i^b \tag{13}$$

$$\tau_i^b = I_i \dot{\omega}_i^b + \omega_i^b \times I_i \omega_i^b \tag{14}$$

A blend of blade element theory and momentum is utilized to derive the quadrotors aerodynamic forces and moments [36]. This is established on the method of G. Fay [37]. The aerodynamic forces and momentums are given in Table 1 [33, 37-40].

For i^{th} quadrotor, Assuming σ_i symbolizes a solidity ratio; λ_i as an inflow ratio; a_i as a lift slope; Y_i as an induced velocity; μ_i as a rotor advance ratio; and ρ_i as an air density.

Table 1. Aerodynamic Forces and Moments.

Forces & Moments	Equations	
Thrust Force	$\begin{cases} T_i = C_{Ti}\,\rho_i A_i \left(\Omega_i R_{radi}\right)^2 \\ \frac{C_{Ti}}{\sigma_i a_i} = \left(\frac{1}{6} + \frac{1}{4}\mu_i^2\right)\theta_{0i} - \left(1 + \mu_i^2\right)\frac{\theta_{t\omega i}}{8} - \frac{1}{4}\lambda_i \end{cases}$	(15)
Hub Force	$\begin{cases} H_i = C_{Hi}\,\rho_i A_i \left(\Omega_i R_{radi}\right)^2 \\ \frac{C_{Hi}}{\sigma_i a_i} = \frac{1}{4a_i}\mu_i \bar{C}_{di} + \frac{1}{4}\lambda_i \mu_i \left(\theta_{0i} - \frac{\theta_{t\omega i}}{2}\right) \end{cases}$	(16)
Drag Moment	$\begin{cases} Q_i = C_{Qi}\,\rho_i A_i \left(\Omega_i R_{radi}\right)^2 R_{radi} \\ \frac{C_{Qi}}{\sigma_i a_i} = \frac{1}{8a_i}\left(1 + \mu_i^2\right)\bar{C}_{di} + \lambda_i \left(\frac{1}{6}\theta_{0i} - \frac{1}{8}\theta_{t\omega i} - \frac{1}{4}\lambda_i\right) \end{cases}$	(17)
Rolling Moment	$\begin{cases} R_{mi} = C_{R_m i}\,\rho_i A_i \left(\Omega_i R_{radi}\right)^2 R_{radi} \\ \frac{C_{R_m i}}{\sigma_i a_i} = -\mu_i \left(\frac{1}{6}\theta_{0i} - \frac{1}{8}\theta_{t\omega i} - \frac{1}{8}\lambda_i\right) \end{cases}$	(18)
Ground Effect	$\dfrac{T_{IGEi}}{T_{OGEi}} = \dfrac{1}{1 - \frac{R_{radi}^2}{16 z_i^2}}$	(19)

2.2. *The relation between "Thrust force and RPM"*

In order to realize a mathematical relation between the rotational speed of the rotor and the produced thrust, a test bench is installed to measure that relation experimentally and derive it in a mathematical form. Figure 2 demonstrates the entire experiment installation.

Figure 2. The test bench installation.

The test bench composed of a hoist tool fastened by a ball bearing to eliminate the friction as possible. A portable electronic digital fishing scale hook suspended with tape mensuration is utilized to measure the weight of the produced thrust. This is installed by fixing one end of the scale whereas the rotor is fixed at the hoist end. A digital photo laser tachometer is utilized to determine the rotational speed of the roller (RPM). An electronic speed controller (ESC) absolutely controls the used brushless DC motor (BLDC) in the experiment by varying the speed of the rotor. For an equivalent portion of time, the ESC varied the speed of the rotor, and the tachometer digital reading measurement is recorded. The experimental results are presented in Table 2.

Table 2. Test Bench Experimental Results.

Current (I) mA	Voltage (v) Volt	Thrust (Mass) N	RPM	Control Effort	PWM %	PWM
0.6	12	0.98	2196	1.625	10%	1100
1.8	12	1.47	2790	3.25	20%	1200
3.6	12	2.646	3600	4.875	30%	1300
5.8	12	3.92	4250	6.5	40%	1400
8.6	12	5.39	4880	8.125	50%	1500
12.6	12	7.056	5500	9.75	60%	1600
17.7	12	8.82	6075	11.375	70%	1700
23.2	12	10.486	6575	13	80%	1800
26	12	10.682	6800	13.8125	85%	1850
28	12	11.172	6850	14.625	90%	1900

The obtained experimental results are utilized to derive a mathematical equation between the thrust and the rotational speed to provoke it in the Simulink/Matlab model. Figure 3 shows that relation. A curve fitting is utilized to get the equation.

$$y = 2.2e\text{-}007*x^2 + 5.1e\text{-}017*x - 1.1e\text{-}013$$
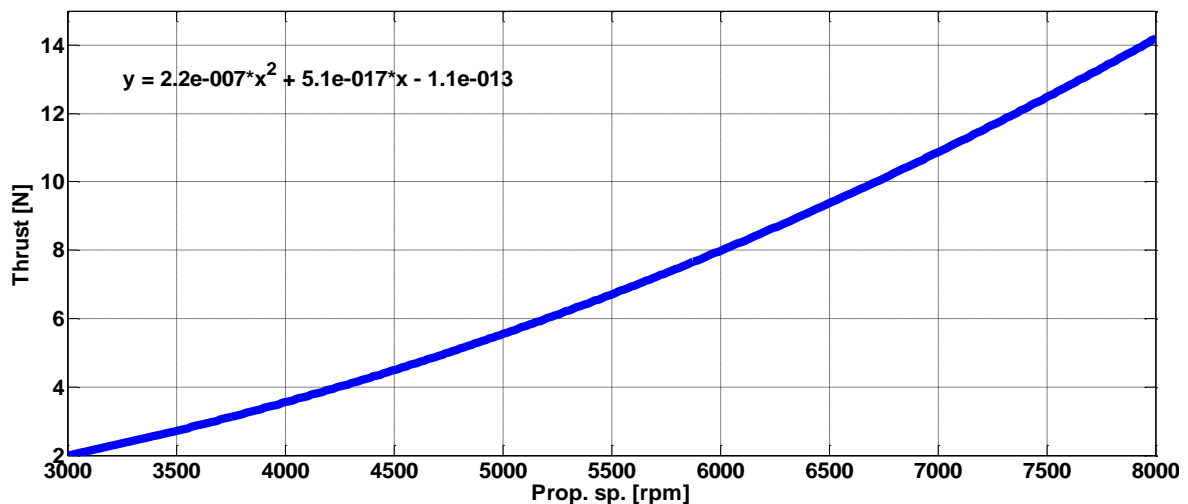
Figure 3. The relation between the thrust and the rotational speed of the rotor.

Using the curve fitting, the relation between the thrust and RPM can be obtained by:

$$T = 2.2e^{-007}\omega^2 + 5.1e^{-017}\omega - 1.1e^{-13} \tag{20}$$

The coefficient of the first order term and the free coefficient are so small to the coefficient of the second order term so it can be neglected, and then the overall thrust force acted on the body-attached structure for n^{th} rotor and i^{th} quadrotor can be determined mathematically from the experimental outcomes to be as in [34]:

$$T_i = \sum_{n=1}^{4} F_{ni} = b_i \sum_{n=1}^{4} \omega_{ni}^2 \tag{21}$$

where T_i is the overall thrust of the quadrotor; F_{ni} is the force generated by the rotor n of quadrotor i ; and ω_i is the rotor speed in RPM.

2.3. Generic Forces and Moments

Quadrotors motion is distinctly accomplished by a combination of forces and moments. Table 3 summarizes the forces and moments acting on i^{th} quadrotor [33].

Table 3. Generic Forces and Momentums.

Forces & Moments		Equations	
Forces along *X*-orientation			
	actuators action	$\left(\sin\phi_i \sin\psi_i + \cos\phi_i \sin\theta_i \cos\psi_i\right)\left(\sum_{n=1}^{4} T_{ni}\right)$	(22)
	hub force in *X*-orientation	$-\sum_{n=1}^{4} H_{xni}$	(23)
	Friction	$\frac{1}{2}C_{xi} A_{ci} \rho_i \dot{x}_i \left|\dot{x}_i\right|$	(24)
Forces along *Y*-orientation			
	actuators action	$\left(-\cos\psi_i \sin\phi_i + \sin\psi_i \sin\theta_i \cos\phi_i\right)\left(\sum_{n=1}^{4} T_{ni}\right)$	(25)
	hub force in *Y*-orientation	$-\sum_{n=1}^{4} H_{yni}$	(26)
	Friction	$\frac{1}{2}C_{yi} A_{ci} \rho_i \dot{y}_i \left|\dot{y}_i\right|$	(27)
Forces along *Z*-orientation			
	actuators action	$\cos\phi_i \cos\psi_i \left(\sum_{n=1}^{4} T_{ni}\right)$	(28)
	Weight	$m_i g$	(29)
Rolling Moment			
	body gyro effect	$\dot{\theta}_i \dot{\psi}_i \left(I_{yyi} - I_{zzi}\right)$	(30)
	propeller gyro effect	$J_{ri} \dot{\theta}_i \Omega_{ri}$	(31)
	roll actuators action	$l_i \left(-T_{2i} + T_{4i}\right)$	(32)
	hub moment due to sideward flight	$h_i \left(\sum_{n=1}^{4} H_{yni}\right)$	(33)
	rolling moment due to forward flight	$(-1)^{n+1} \sum_{n=1}^{4} R_{mxni}$	(34)
Pitching Moment			
	body gyro effect	$\dot{\phi}_i \dot{\psi}_i \left(I_{zzi} - I_{xxi}\right)$	(35)

propeller gyro effect	$J_{ri}\dot{\phi}_i\Omega_{ri}$	(36)
pitch actuators action	$l_i\left(T_{1i}-T_{3i}\right)$	(37)
hub moment due to forward flight	$h_i\left(\sum\limits_{n=1}^{4}H_{xni}\right)$	(38)
rolling moment due to sideward flight	$(-1)^{n+1}\sum\limits_{n=1}^{4}R_{myni}$	(39)

Yawing Moment

body gyro effect	$\dot{\phi}_i\dot{\theta}_i\left(I_{xxi}-I_{yyi}\right)$	(40)
inertial counter-torque	$J_{ri}\dot{\Omega}_{ri}$	(41)
counter-torque unbalance	$(-1)^{n}\sum\limits_{n=1}^{4}Q_{ni}$	(42)
hub unbalance in forward flight	$l_i\left(H_{x2i}-H_{x4i}\right)$	(43)
rolling moment due to forward flight	$l_i\left(-H_{y1i}+H_{y3i}\right)$	(44)

2.4. Quadrotor Equation of Motion

Quadrotors equation of motion can be proved from (13), (14), and all prior listed equation of forces and moments as [41]:

$$
\begin{cases}
\ddot{x}_i = \dfrac{1}{m_i}\left[\left(\sin\theta_i\cos\phi_i\cos\psi_i+\sin\phi_i\sin\psi_i\right)\sum\limits_{n=1}^{4}T_{ni}-\sum\limits_{n=1}^{4}H_{xni}-\tfrac{1}{2}\rho_iA_{ci}C_{xi}\dot{x}_i\left|\dot{x}_i\right|\right] \\[2mm]
\ddot{y}_i = \dfrac{1}{m_i}\left[\left(\sin\theta_i\cos\phi_i\sin\psi_i-\sin\phi_i\cos\psi_i\right)\sum\limits_{n=1}^{4}T_{ni}-\sum\limits_{n=1}^{4}H_{yni}-\tfrac{1}{2}\rho_iA_{ci}C_{yi}\dot{y}_i\left|\dot{y}_i\right|\right] \\[2mm]
\ddot{z}_i = \dfrac{1}{m_i}\left[m_ig-\left(\cos\phi_i\cos\psi_i\right)\sum\limits_{n=1}^{4}T_{ni}\right] \\[2mm]
\ddot{\phi}_i = \dfrac{1}{I_{xxi}}\left[\dot{\theta}_i\dot{\psi}_i\left(I_{yyi}-I_{zzi}\right)+\Omega_{ri}J_{ri}\dot{\theta}_i+l_i\left(-T_{2i}+T_{4i}\right)-h_i\sum\limits_{n=1}^{4}H_{yni}+(-1)^{n+1}\sum\limits_{n=1}^{4}R_{mxni}\right] \\[2mm]
\ddot{\theta}_i = \dfrac{1}{I_{yyi}}\left[\dot{\phi}_i\dot{\psi}_i\left(I_{zzi}-I_{xxi}\right)+\Omega_{ri}J_{ri}\dot{\phi}_i+l_i\left(T_{1i}-T_{3i}\right)+h_i\sum\limits_{n=1}^{4}H_{xni}+(-1)^{n+1}\sum\limits_{n=1}^{4}R_{myni}\right] \\[2mm]
\ddot{\psi}_i = \dfrac{1}{I_{zzi}}\left[\dot{\phi}_i\dot{\theta}_i\left(I_{xxi}-I_{yyi}\right)+\Omega_{ri}J_{ri}+(-1)^{n}\sum\limits_{n=1}^{4}Q_{ni}+l_i\left(H_{x2i}-H_{x4i}\right)+l_i\left(-H_{y1i}+H_{y3i}\right)\right]
\end{cases}
\tag{45}
$$

For simplicity, the quadrotors equation of motion in (45) may be rewritten as [33]:

$$
\begin{cases}
\ddot{x}_i = \sum F_{xi} / m_i \\[2ex]
\ddot{y}_i = \sum F_{yi} / m_i \\[2ex]
\ddot{z}_i = g - \sum F_{zi} / m_i \\[2ex]
\ddot{\phi}_i = \sum \tau_{xi} / I_{xxi} \\[2ex]
\ddot{\theta}_i = \sum \tau_{yi} / I_{yyi} \\[2ex]
\ddot{\psi}_i = \sum \tau_{zi} / I_{zzi}
\end{cases}
\tag{46}
$$

2.5. Modelling for Control

For the control simplicity, the exact complete model of the quadrotor is simplified by reducing the external forces and the external torques to adhere to the real-time limitations of the embedded control loop [40]. Therefore, the quadrotor system i with 6-DOF and 12-states can be rephrased in state-space formulation $\dot{X}_i = f(X_i, U_i)$ considering the inputs vector U_i and the state vector X_i of the system such that [39]:

$$
X_i = [\phi_i, \dot{\phi}_i, \theta_i, \dot{\theta}_i, \psi_i, \dot{\psi}_i, z_i, \dot{z}_i, x_i, \dot{x}_i, y_i, \dot{y}_i]^T
\tag{47}
$$

Assuming

$$
\begin{aligned}
&x_{1i} = \phi_i & &x_{7i} = z_i \\
&x_{2i} = \dot{x}_{1i} = \dot{\phi}_i & &x_{8i} = \dot{x}_{7i} = \dot{z}_i \\
&x_{3i} = \theta_i & &x_{9i} = x_i \\
&x_{4i} = \dot{x}_{3i} = \dot{\theta}_i & &x_{10i} = \dot{x}_{9i} = \dot{x}_i \\
&x_{5i} = \psi_i & &x_{11i} = y_i \\
&x_{6i} = \dot{x}_{5i} = \dot{\psi}_i & &x_{12i} = \dot{x}_{11i} = \dot{y}_i
\end{aligned}
\tag{48}
$$

$$
U_i = \begin{bmatrix} U_{1i} & U_{2i} & U_{3i} & U_{4i} \end{bmatrix}^T
\tag{49}
$$

The inputs can be mapped as [42]:

$$
\begin{cases}
U_{1i} = K_{Ti} \sum_{n=1}^{4} \Omega_{ni}^2 \\[2ex]
U_{2i} = K_{Ti} (\Omega_{1i}^2 - \Omega_{3i}^2) \\[1ex]
U_{3i} = K_{Ti} (\Omega_{2i}^2 - \Omega_{4i}^2) \\[1ex]
U_{4i} = K_{Di} (\Omega_{2i}^2 + \Omega_{4i}^2 - \Omega_{1i}^2 - \Omega_{3i}^2)
\end{cases}
\tag{50}
$$

From (47) and (49):

$$
f\left(X_i, U_i\right) =
\begin{pmatrix}
\dot{\phi}_i \\
\dot{\theta}_i \dot{\psi}_i a_{1i} + \dot{\theta}_i a_{2i} \Omega_{ri} + b_{1i} U_{2i} \\
\dot{\theta}_i \\
\dot{\phi}_i \dot{\psi}_i a_{3i} - \dot{\phi}_i a_{4i} \Omega_{ri} + b_{2i} U_{3i} \\
\dot{\psi}_i \\
\dot{\phi}_i \dot{\theta}_i a_{5i} + b_{3i} U_{4i} \\
\dot{z}_i \\
g - \frac{1}{m_i}(\cos\phi_i \cos\theta_i) U_{1i} \\
\dot{x}_i \\
u_{xi} \frac{1}{m_i} U_{1i} \\
\dot{y}_i \\
u_{yi} \frac{1}{m_i} U_{1i}
\end{pmatrix}
\tag{51}
$$

where

$$
\begin{cases}
a_{1i} = (I_{yi} - I_{zi})/I_{xi} & a_{2i} = -J_{ri}/I_{xi} \\
a_{3i} = (I_{zi} - I_{xi})/I_{yi} & a_{4i} = J_{ri}/I_{yi} \\
a_{5i} = (I_{xi} - I_{yi})/I_{zi} & b_{1i} = l_i/I_{xi} \\
b_{2i} = l_i/I_{yi} & b_{3i} = 1/I_{zi}
\end{cases}
\tag{52}
$$

$$
\begin{cases}
u_{xi} = \cos\phi_i \sin\theta_i \cos\psi_i + \sin\phi_i \sin\psi_i \\
u_{yi} = \cos\phi_i \sin\theta_i \sin\psi_i - \sin\phi_i \cos\psi_i
\end{cases}
\tag{53}
$$

From (51), the rotational rate of the quadrotor can be outlined as:

$$
\begin{pmatrix}
\dot{x}_{2i} \\
\dot{x}_{4i} \\
\dot{x}_{6i}
\end{pmatrix}
=
\begin{pmatrix}
a_{1i} x_{4i} x_{6i} + a_{2i} x_{4i} \Omega_{ri} + b_{1i} U_{2i} \\
a_{3i} x_{2i} x_{6i} + a_{4i} x_{2i} \Omega_{ri} + b_{2i} U_{3i} \\
a_{5i} x_{2i} x_{4i} + b_{3i} U_{4i}
\end{pmatrix}
\tag{54}
$$

Equations (50) and (54) enable designing the attitude control of the quadrotor. Neglecting the gyroscopic terms in (54):

$$
\begin{pmatrix}
\dot{x}_{2i} \\
\dot{x}_{4i} \\
\dot{x}_{6i}
\end{pmatrix}
=
\begin{pmatrix}
a_{1i} x_{4i} x_{6i} + b_{1i} U_{2i} \\
a_{3i} x_{2i} x_{6i} + b_{2i} U_{3i} \\
a_{5i} x_{2i} x_{4i} + b_{3i} U_{4i}
\end{pmatrix}
\tag{55}
$$

Assuming U_{2i}^*, U_{3i}^* and U_{4i}^* to get a linear system where:

$$
\begin{cases}
U_{2i} = f_{2i}\left(x_{2i}, x_{4i}, x_{6i}\right) + U_{2i}^* \\
U_{3i} = f_{3i}\left(x_{2i}, x_{4i}, x_{6i}\right) + U_{3i}^* \\
U_{4i} = f_{4i}\left(x_{2i}, x_{4i}, x_{6i}\right) + U_{4i}^*
\end{cases}
\tag{56}
$$

Fulfilling the upcoming equation:

$$\begin{cases} a_{1i}x_{4i}x_{6i}+b_{1i}f_{2i}(x_{2i},x_{4i},x_{6i})=K_{2i}x_{2i} \\ a_{3i}x_{2i}x_{6i}+b_{2i}f_{3i}(x_{2i},x_{4i},x_{6i})=K_{3i}x_{4i} \\ a_{5i}x_{2i}x_{4i}+b_{3i}f_{4i}(x_{2i},x_{4i},x_{6i})=K_{4i}x_{6i} \end{cases} \tag{57}$$

The nonlinear feedback for linearization can be obtained by:

$$\begin{cases} f_{2i}(x_{2i},x_{4i},x_{6i})=\frac{1}{b_{1i}}(K_{2i}x_{2i}-a_{1i}x_{4i}x_{6i}) \\ f_{3i}(x_{2i},x_{4i},x_{6i})=\frac{1}{b_{2i}}(K_{3i}x_{4i}-a_{3i}x_{2i}x_{6i}) \\ f_{4i}(x_{2i},x_{4i},x_{6i})=\frac{1}{b_{3i}}(K_{4i}x_{6i}-a_{5i}x_{2i}x_{4i}) \end{cases} \tag{58}$$

Utilizing (58) yields transformation of (55) to the linear and decoupled system as:

$$\begin{pmatrix} \dot{x}_{2i} \\ \dot{x}_{4i} \\ \dot{x}_{6i} \end{pmatrix} = \begin{pmatrix} K_{2i}x_{2i}+\frac{1}{b_{1i}}U_{2i}^{*} \\ K_{3i}x_{4i}+\frac{1}{b_{2i}}U_{3i}^{*} \\ K_{4i}x_{6i}+\frac{1}{b_{3i}}U_{4i}^{*} \end{pmatrix} \tag{59}$$

Considering $U_{2i}^{*}=U_{3i}^{*}=U_{4i}^{*}=0$ and the operating point $x_{2i}=x_{4i}=x_{6i}=0$; the produced the linearized closed-loop order is steady alike with the presence or absence of the gyroscopic term in (54). Confirming that point will be proved by assuming the Lyapunov function $V_i(x_{2i},x_{4i},x_{6i})$ for the attitude controller G_{ci} and positive designated about the operating point:

$$V_i(x_{2i},x_{4i},x_{6i})=0.5(x_{2i}^{2}+x_{4i}^{2}+x_{6i}^{2}) \tag{60}$$

The first derivative of the Lyapunov function $\dot{V}_i$ is determined by utilizing (54), (56), and (58). Moreover; if $a_{1i}=-a_{3i}$ and $a_{5i}=0$, a typical cross configuration of the quadrotor with $I_{xi}=I_{yi}$ is resulted. So, $\dot{V}_i$ can be obtained by:

$$\begin{aligned} \dot{V}_i &= x_{2i}\dot{x}_{2i}+x_{4i}\dot{x}_{4i}+x_{6i}\dot{x}_{6i} \\ &= K_{2i}x_{2i}^{2}+K_{3i}x_{4i}^{2}+K_{4i}x_{6i}^{2} \end{aligned} \tag{61}$$

It is clear that $\dot{V}_i$ is also free from gyroscopic terms. $\dot{V}_i$ is negative if $K_{2i},K_{3i},K_{4i}<0$. So, the operating point of the feedback linearized order is asymptotically stable.

$$\begin{pmatrix} \ddot{x}_{1i} \\ \ddot{x}_{3i} \\ \ddot{x}_{5i} \end{pmatrix} = \begin{pmatrix} K_{2i}\dot{x}_{1i}+\frac{1}{b_{1i}}U_{2i}^{*} \\ K_{3i}\dot{x}_{3i}+\frac{1}{b_{2i}}U_{3i}^{*} \\ K_{4i}\dot{x}_{5i}+\frac{1}{b_{3i}}U_{4i}^{*} \end{pmatrix} \tag{62}$$

If x_{1id},x_{3id},x_{5id} are the required angels, utilization of the linear controller:

$$\begin{cases} U_{2i}^{*}=w_{2i}\cdot(x_{1id}-x_{1i}) \\ U_{3i}^{*}=w_{3i}\cdot(x_{3id}-x_{3i}) \\ U_{4i}^{*}=w_{4i}\cdot(x_{5id}-x_{5i}) \end{cases} \tag{63}$$

Submitting (63) into (62) and transforming the system from the time domain to s domain by applying Laplace transformation on (62) yields a second-order transfer function:

$$\begin{cases} F_{1i} = \dfrac{X_{1i}(s)}{X_{1id}(s)} = \dfrac{w_{2i}}{\frac{1}{b_{1i}}s^2 - \frac{K_{2i}}{b_{1i}}s + \omega_{2i}} \\[3ex] F_{3i} = \dfrac{X_{3i}(s)}{X_{3id}(s)} = \dfrac{w_{3i}}{\frac{1}{b_{2i}}s^2 - \frac{K_{3i}}{b_{2i}}s + \omega_{3i}} \\[3ex] F_{5i} = \dfrac{X_{5i}(s)}{X_{5id}(s)} = \dfrac{w_4}{\frac{1}{b_{3i}}s^2 - \frac{K_{4i}}{b_{3i}}s + \omega_{4i}} \end{cases} \tag{64}$$

Adjusting the pair of coefficients $(K_{2i}, w_{2i}), (K_{3i}, w_{3i}), (K_{4i}, w_{4i})$ respectively enable controlling these closed-loop quadrotors systems. The coefficients K_{2i}, K_{3i}, K_{4i} should be negative as a restriction along with the restriction from the hardware sides particularly the consideration of the motor torque.

3. Quadrotors Control Approaches

3.1. *PID Control Design*

PID controllers are ordinarily utilized, seeing manufacturing controlled systems, according to the decreased number of tuned coefficients [43-45], and design simplicity [16]. It is recorded that more than 90% of implemented controllers are regularly based on PID controllers [46, 47]. PID controller is created to control every quadrotor of a team of cooperative quadrotors. The controller manipulated system error produced by the control system. PID controller consists of various triple coefficients to earn the optimum output from the controller [48]. The general form of PID controller is formulated as in (65) [49]:

$$u(t) = K_P + K_I \int_0^t e(t)dt + K_D \frac{d}{dt}e(t) \tag{65}$$

A block schematic diagram for a system with (PID) control is shown in Figure 4.
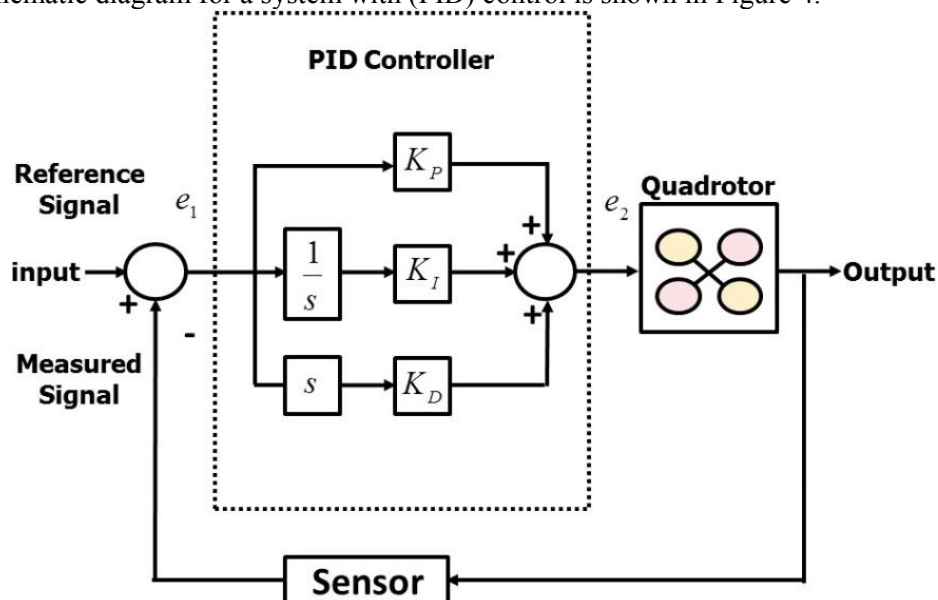
Figure 4. A block schematic diagram for a quadrotor with PID control.

To create a simple inverse model that can be executed in the control techniques, the quadrotor dynamics should be simplified. The dynamic model can be readjusted by dropping the gyroscopic and Coriolis-centripetal terms.

The simplified model can be rewritten as follows:

$$
\begin{pmatrix} \ddot{x}_{1i} \\ \ddot{x}_{3i} \\ \ddot{x}_{5i} \end{pmatrix} = \begin{pmatrix} \ddot{\phi}_i \\ \ddot{\theta}_i \\ \ddot{\psi}_i \end{pmatrix} = \begin{pmatrix} \dfrac{l_i}{I_{xxi}} U_{2i} \\[2ex] \dfrac{l_i}{I_{yyi}} U_{3i} \\[2ex] \dfrac{1}{I_{zzi}} U_{4i} \end{pmatrix}
\tag{66}
$$

Inserting the rotor dynamics in (66) and reforming the model in Laplace domain as:

$$
\begin{cases}
\phi_i(s) = \dfrac{B_i^2 b_i l_i}{s^2 (s+A_i)^2 I_{xxi}} \left(u_{4i}^2(s) - u_{2i}^2(s) \right) \\[3ex]
\theta_i(s) = \dfrac{B_i^2 b_i l_i}{s^2 (s+A_i)^2 I_{yyi}} \left(u_{3i}^2(s) - u_{1i}^2(s) \right) \\[3ex]
\psi_i(s) = \dfrac{A_i^2}{s^2 (s+A_i)^2 I_{zzi}} \sum_{n=1}^{4} (-1)^{n+1} u_{ni}^2(s)
\end{cases}
\tag{67}
$$

where, the coefficients A_i and B_i represent the rotor dynamics. By replacing the motor inputs by the control inputs; (50) becomes:

$$
\begin{cases}
\phi_i(s) = \dfrac{A_i^2 l_i}{s^2 (s+A_i)^2 I_{xxi}} U_{2i} \\[3ex]
\theta_i(s) = \dfrac{A_i^2 l_i}{s^2 (s+A_i)^2 I_{yyi}} U_{3i} \\[3ex]
\psi_i(s) = \dfrac{A_i^2}{s^2 (s+A_i)^2 I_{zzi}} U_{4i}
\end{cases}
\tag{68}
$$

Eventually, the controller equations can be obtained as in (69):

$$
\begin{cases}
U_{2i} = \dfrac{1}{b_{1i}} (K_{2i} x_{2i} - a_{1i} x_{4i} x_{6i}) + w_{2i} (x_{1id} - x_{1i}) \\[3ex]
U_{3i} = \dfrac{1}{b_{2i}} (K_{3i} x_{4i} - a_{3i} x_{2i} x_{6i}) + w_{3i} (x_{3id} - x_{3i}) \\[3ex]
U_{4i} = \dfrac{1}{b_{3i}} (K_{4i} x_{6i} - a_{5i} x_{4i} x_{6i}) + w_{4i} (x_{5id} - x_{5i})
\end{cases}
\tag{69}
$$

where $x_{2i} = \dot{\phi}_i, x_{4i} = \dot{\theta}_i, x_{6i} = \dot{\psi}_i$,   and $x_{1id}, x_{3id}, x_{5id}$ are the desired angles and $x_{1id} = x_{3id} = x_{5id} = 0$ in case of the hovering state.

This controller can be readily implemented. The upcoming challenge in the design procedure is the choice of the controller coefficients values of $(K_{2i}, w_{2i}), (K_{3i}, w_{3i}), (K_{4i}, w_{4i})$. The simplex optimization algorithm is used to get the optimum values of these controller coefficients as elementary acceptable coefficient values for the genetic algorithm (GA). Fine adjusting of PID coefficients is acquired utilizing GA which is a hypothetical evolutionary method with a similar analogy to the actual world biology. Selection of the parents and the conjunction of their genes to generate the posterior generation (crossover) is a fundamental procedure for the GA [50]. The genetic algorithm is intended

to reduce the multi-objective function. This function reduces the mean square error (MSE) amidst the reference input and the output of the system without overshoot [51-53]. The utilized coefficients by the genetic algorithm toolbox in Matlab are shown in Table 4.

Table 4. Genetic Algorithm Coefficients.

Population size	Crossover	Number of generations
200	0.8	800

It is noted that every control technique is dedicated to the objective of performance optimization of a particular subsystem [54]. The objectives of the optimization operation are realizing the stability performance for the cooperative quadrotors, faster response, and decreasing overshoots as minimum as possible.

A PD controller is designed for every orientation angle. The nonlinear feedback controller has the form shown in (70):

$$U_{2i,3i,4i} = K_{pi_{\phi_i,\theta_i,\psi_i}}(\phi_i,\theta_i,\psi_i) + K_{Di_{\phi_i,\theta_i,\psi_i}}(\dot{\phi}_i,\dot{\theta}_i,\dot{\psi}_i) \tag{70}$$

To get the desired behavior of the altitude control for the vertical position, the upcoming control law is applied:

$$u_{1i} = \frac{r_{1i} + m_i g}{\cos\phi_i \cos\theta_i} \tag{71}$$

$$r_{1i} = -a_{1i}\dot{z}_i - a_{2i}(z_i - z_{id}) \tag{72}$$

The desired altitude z_d can be calculated by:

$$z_{id} = \frac{-a_{1i}\dot{z}_i - a_{2i}z_i - r_{1i}}{a_{2i}} \tag{73}$$

The coefficients a_{1i} and a_{2i} are representing K_{Di} and K_{pi} respectively. These coefficients should be positive. Considering the hardware limitation and the noise effect with the controller parameters has been chosen as shown in Table 5:

Table 5. PD controller coefficients.

Controller Gain	Roll	Pitch	Yaw	Altitude
K_{Pi}	-14.6211	-46.6211	-64	4.7673
K_{Di}	48.7832	112.7832	42.2144	4.9794

Several simulation experiments are conducted to validate the underlying control law. The controller achieved successfully several simulation experiments even with sever initial conditions on the attitude channels.

3.2. *Backstepping Control Design*

Backstepping control technique has already been investigated in [41]. Backstepping controller technique is a favored regulator over several controller techniques. It uses a recursive algorithm, where the controller has divided its mechanism into several steps guaranteeing the stability of each step gradually [15]. Backstepping ensures asymptotic robustness, stability, observability, and controllability [55].

Backstepping controller fetches the data from the sensors straight with the assigned mission as inputs. The controller uses many parameters during the calculation. These parameters represent the states and the dynamics of the quadrotors. The output of the algorithm is the code that allocates the PWM signal for each motor of the four motors of each quadrotor.

Backstepping control is chosen to provide angular controls of the i_{th} quadrotor airplane in which the inputs U_{2i}, U_{3i} and U_{4i} control quadrotor aerial robot at hovering, where $i = 1, 2, ..., j$ (j is the number of quadrotor in the swarming team).

The desired control U_{2i} is identified as [41]:

$$U_{2i} = \frac{I_{yi}}{l} \left[-\left(k_{1i}^2 + \frac{c_{1i} k_{2i}}{k_{1i}} + c_{1i} c_{2i} + \frac{c_{2i} k_{2i}}{k_{1i}} \right) e_i - \left(c_{1i} + \frac{k_{2i}}{k_{1i}} + c_{2i} \right) \dot{e}_i - \left(\frac{I_{zi} - I_{xi}}{I_{yi}} \right) \dot{\phi}_i \dot{\psi}_i \right.$$
$$\left. - \left(k_{1i} k_{2i} + \frac{c_{1i} c_{2i} k_{2i}}{k_{1i}} \right) \int e_i dt + \ddot{\phi}_{di} \right] \qquad (74)$$

From (65), U_{2i} is a backstepping control and its gains are:

$$K_{Pi} = \left(k_{1i}^2 + \frac{c_{1i} k_{2i}}{k_{1i}} + c_{1i} c_{2i} + \frac{c_{2i} k_{2i}}{k_{1i}} \right), K_{Ii} = \left(k_{1i} k_{2i} + \frac{c_{1i} c_{2i} k_{2i}}{k_{1i}} \right), \text{ and } K_{Di} = \left(c_{1i} + \frac{k_{2i}}{k_{1i}} + c_{2i} \right) \quad (75)$$

Similarly, U_{3i} and U_{4i} as in Eq. (76) and Eq. (77):

$$U_{3i} = \frac{I_{xi}}{l} \left[-\left(k_{3i}^2 + \frac{c_{3i} k_{4i}}{k_{3i}} + c_{3i} c_{4i} + \frac{c_{4i} k_{4i}}{k_{3i}} \right) e_i - \left(c_{3i} + \frac{k_{4i}}{k_{3i}} + c_{4i} \right) \dot{e}_i - \left(\frac{I_{yi} - I_{zi}}{I_{xi}} \right) \dot{\theta}_i \dot{\psi}_i \right.$$
$$\left. - \left(k_{3i} k_{4i} + \frac{c_{3i} c_{4i} k_{4i}}{k_{3i}} \right) \int e_i dt + \ddot{\theta}_{di} \right] \qquad (76)$$

$$U_{4i} = \frac{I_{zi}}{l} \left[-\left(k_{5i}^2 + \frac{c_{5i} k_{6i}}{k_{5i}} + c_{5i} c_{6i} + \frac{c_{6i} k_{6i}}{k_{5i}} \right) e_i - \left(k_{5i} k_{6i} + \frac{c_{5i} c_{6i} k_{6i}}{k_{5i}} \right) \int e_i dt - \left(c_{5i} + \frac{k_{6i}}{k_{5i}} + c_{6i} \right) \dot{e}_i + \ddot{\psi}_{di} \right] \qquad (77)$$

4. Quadrotors Control Approaches

Various simulations experiments on Matlab Simulink are conducted utilizing the whole model to adjust the control coefficients. The controller's function is designed to stabilize the orientation angles for every quadrotor of a team of cooperative quadrotors. For these simulations, the dynamic model is utilized without considering the measurement noise. $\dot{\phi}_i, \dot{\theta}_i, \dot{\psi}_i$ coefficients are acquired from the gyros, and then ϕ_i, θ_i, ψ_i coefficients are determined by integrating the values of rate of change for every controlled channel acquired from the gyros. The separating spans and velocity are constrained in the control designing. The designed trajectory tracking, noise cancellation, and wind disturbance rejection are deemed as a comparison criterion between the two controllers. A couple of scenarios in obstacle-free and obstacle-laden surroundings is supposed.

4.1. *Scenario 1 (obstacle-free surroundings):*
The cooperative quadrotors are tested in trajectory tracking with and without noise and wind disturbance effect as shown in the upcoming figures. Figure 5 displays the trajectory tracking of the cooperative quadrotors (Leaders and followers) controlled by PID and backstepping controllers in *X*-orientation and compares between the obtained results. The results show approximately identical trajectory tracking of the cooperative quadrotors in *X*-orientation using both PID and backstepping controllers.
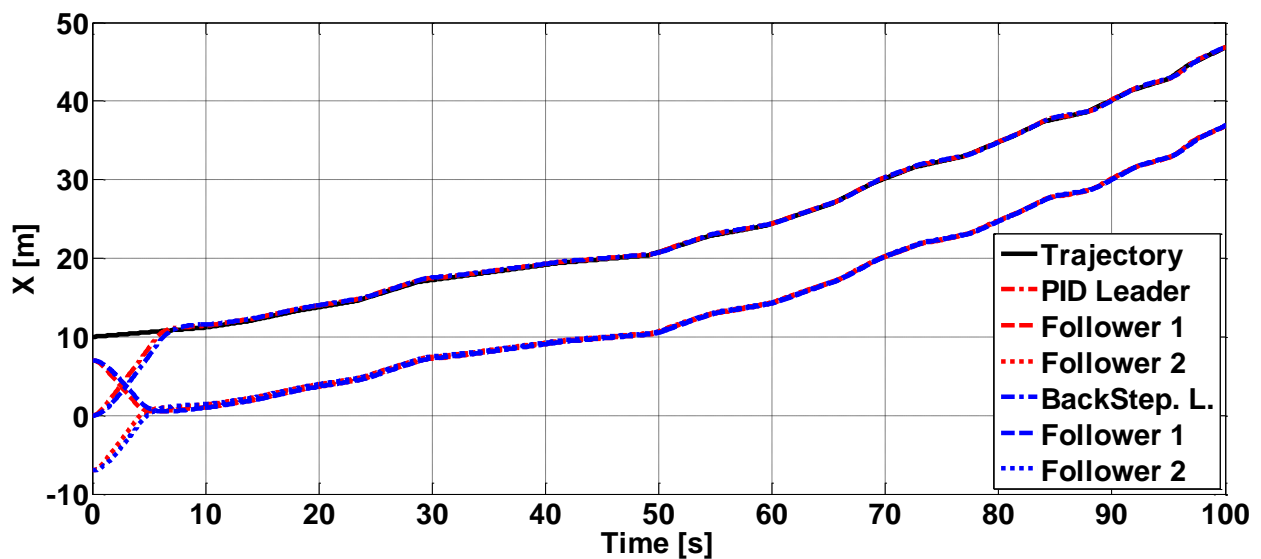
Figure 5. The trajectory tracking of the cooperative quadrotors controlled by PID and backstepping controllers in *X*-orientation.

Figure 6 shows the trajectory tracking of the cooperative quadrotors (Leaders and followers) controlled by PID and backstepping controllers in *Y*-orientation and compares between the obtained results. The results show approximately identical trajectory tracking of the cooperative quadrotors in *Y*-orientation using both PID and backstepping controllers.
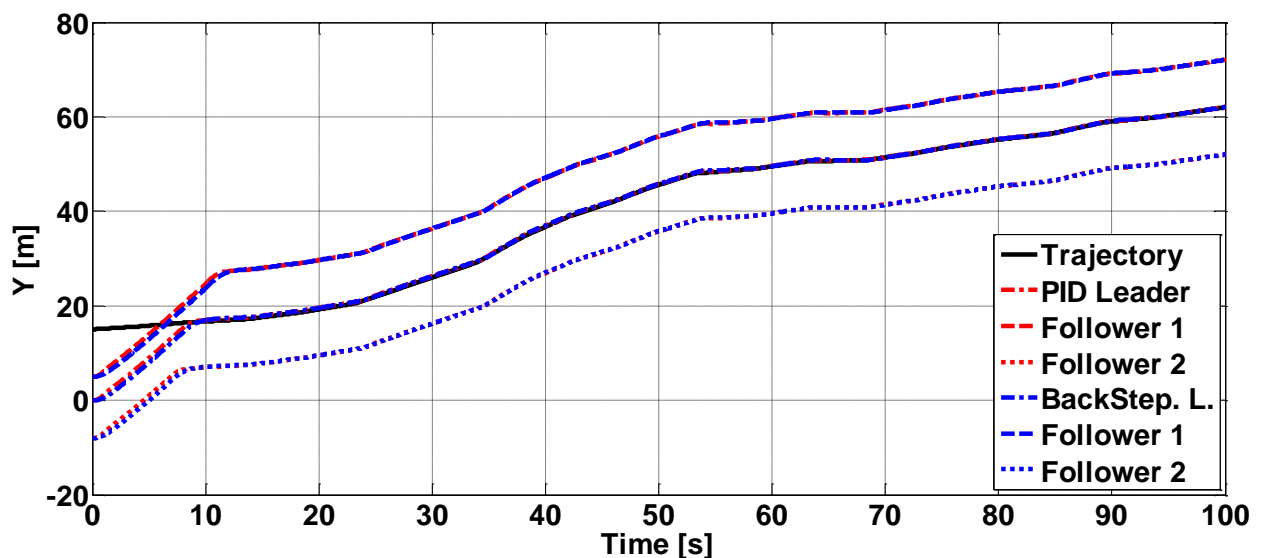
Figure 6. The trajectory tracking of the cooperative quadrotors controlled by PID and backstepping controllers in *Y*-orientation.

Figure 7 shows the trajectory tracking of the cooperative quadrotors (Leaders and followers) controlled by PID and backstepping controllers in *XY*-plane and compares between the obtained results. The results show approximately identical trajectory tracking of the cooperative quadrotors in *XY*-plane using both PID and backstepping controllers.
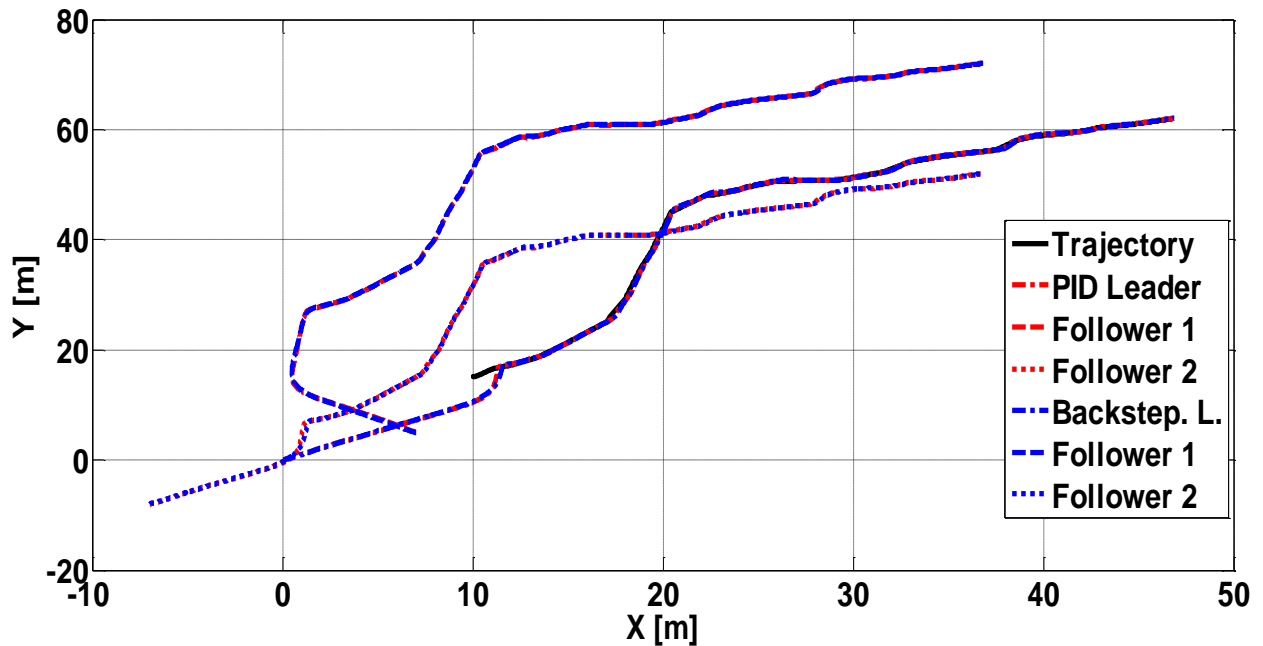
Figure 7. The trajectory tracking of the cooperative quadrotors controlled by PID and backstepping controllers in *XY*-plane.

Figure 8, and Figure 9 show the separating span between the team of the cooperative quadrotors in *X*-orientation and *Y*-orientation respectively using the PID controller. The same figures can be obtained using the backstepping controller because of identical trajectory tracking in *XY*-plane for both types of controllers.
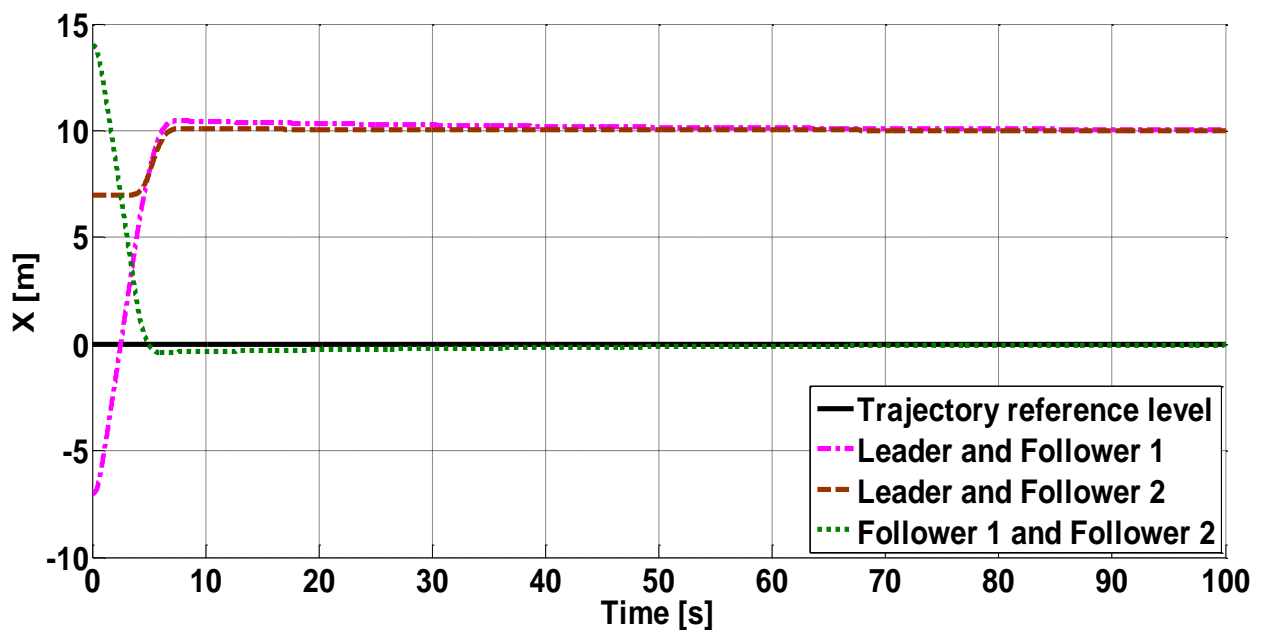
Figure 8. Separating span between the team of the cooperative quadrotors in *X*-orientation.
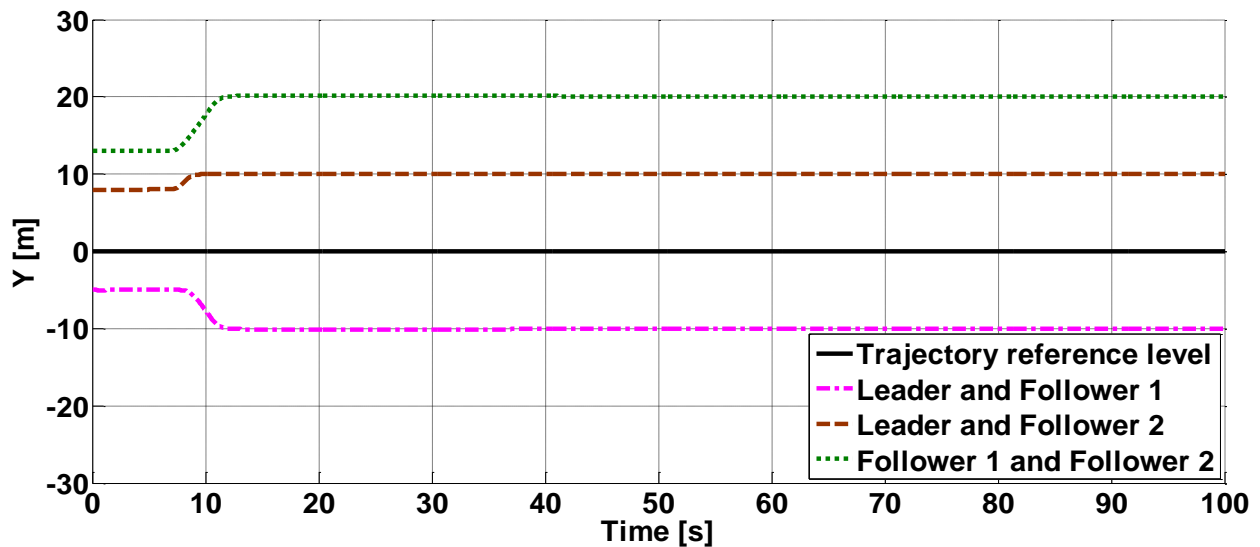
Figure 9. Separating span between the team of the cooperative quadrotors in *Y*-orientation.

Figure 10 shows the trajectory tracking of the cooperative quadrotors (Leaders and followers) controlled by PID and backstepping controllers in *Z*-orientation and compares between the obtained results. The results obtained show that the output response of the cooperative quadrotors controlled using PID controller is faster than that of cooperative quadrotors controlled using the backstepping controller in *Z*-orientation. The output response of the cooperative quadrotors controlled using PID controller has small overshoot which does not exist in the output response of the cooperative quadrotors controlled using the backstepping controller. Only one curve is presented for the cooperative quadrotors in every figure because the leader and the followers have the same altitude.
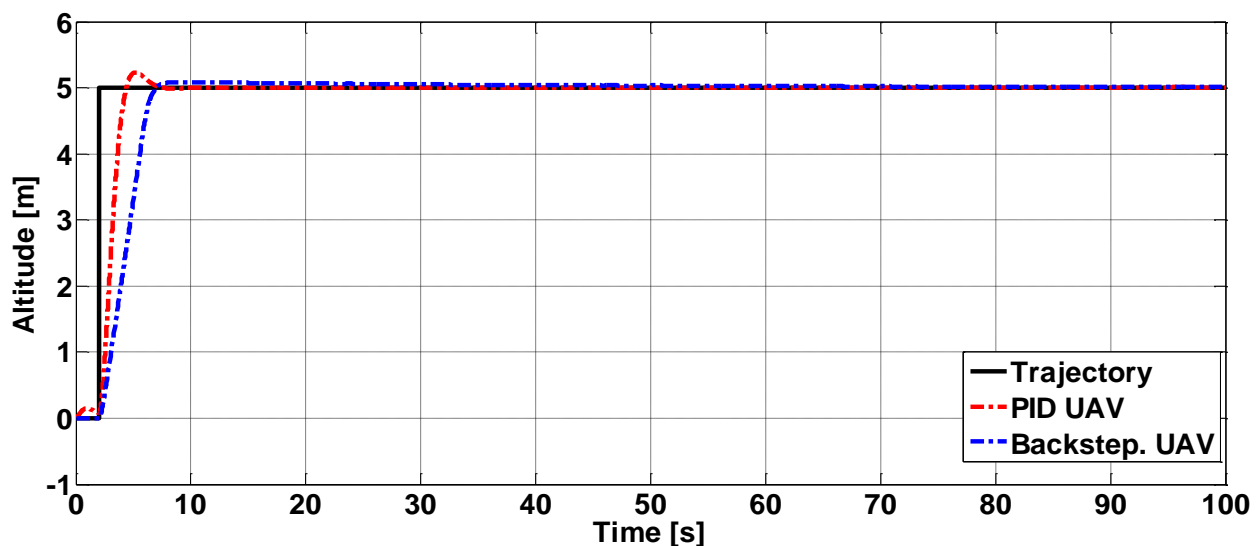
Figure 10. The trajectory tracking of the cooperative quadrotors controlled by PID and backstepping controllers in *Z*-orientation.

Figure 11 shows the trajectory tracking of the cooperative quadrotors (Leaders and followers) controlled by PID and backstepping controllers in *XYZ*-space and compares between the obtained results. The results show that the cooperative quadrotors controlled using PID controller reach the desired altitude faster than cooperative quadrotors controlled using the backstepping controller. Approximately identical path obtained for the cooperative quadrotors in *XY*-plane after reaching the desired altitude using both PID and backstepping controllers.
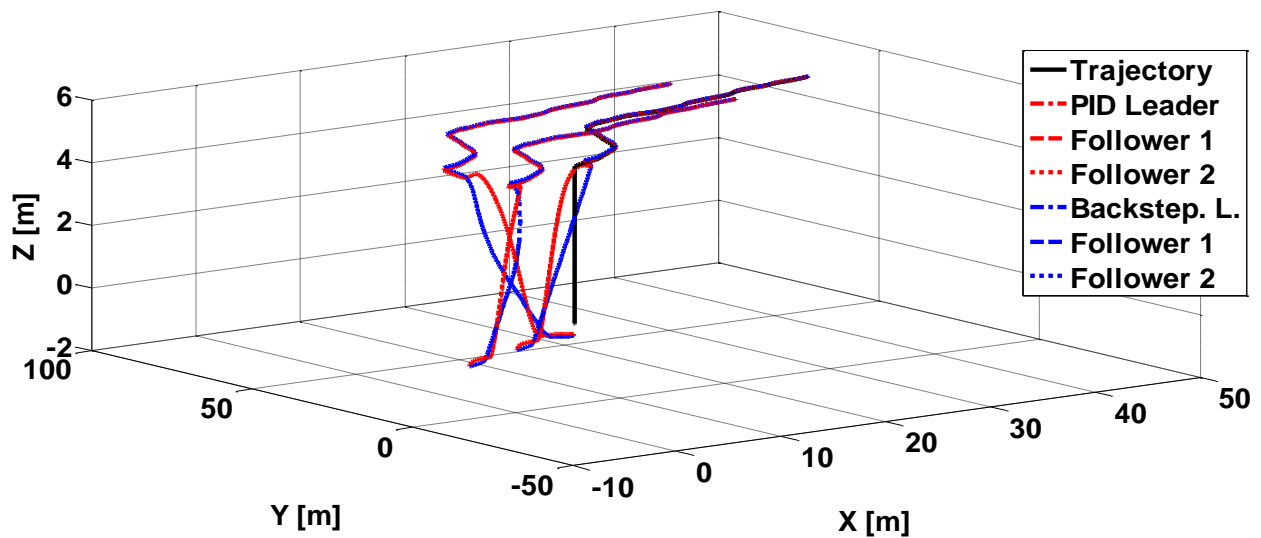
Figure 11. The trajectory tracking of the cooperative quadrotors controlled by PID and backstepping controllers in *XYZ*-space.

4.2. Scenario 2 (*obstacle-laden surroundings*):

The obstacle avoidance algorithm has already been investigated in [41]. The proposed obstacle is created as a rectangle appearing in the simulation as a plan view of an obstacle. The quadrotors altitudes are given as a constant level through the obstacle avoidance process in the simulation. For aviation security issues; a couple of safety zones are always preserved with 20m-radius safety zone and 10m-separating span named as a shielded zone amidst every follower and the leader of the team [56]. These zones guarantee a 20m-radius initially to launch the manoeuvre at the border of this safety zone amidst the team quadrotors and any obstacle. If an obstacle is sensed on the border of the safety zone, a rescue loop is initiated causing trajectory tracking obstruction, then a wily manoeuvre in a half circle path to avert the obstacle and then returning to track the main trajectory.

Figure 12 shows the trajectory tracking of a straight line and obstacle avoidance of the cooperative quadrotors (Leaders and followers) controlled by PID and backstepping controllers in *XY*-plane and compares between the obtained results. The results show that the cooperative quadrotors controlled using PID controller take larger curvature when dealing with obstacle avoidance than it takes by cooperative quadrotors controlled using the backstepping controller.
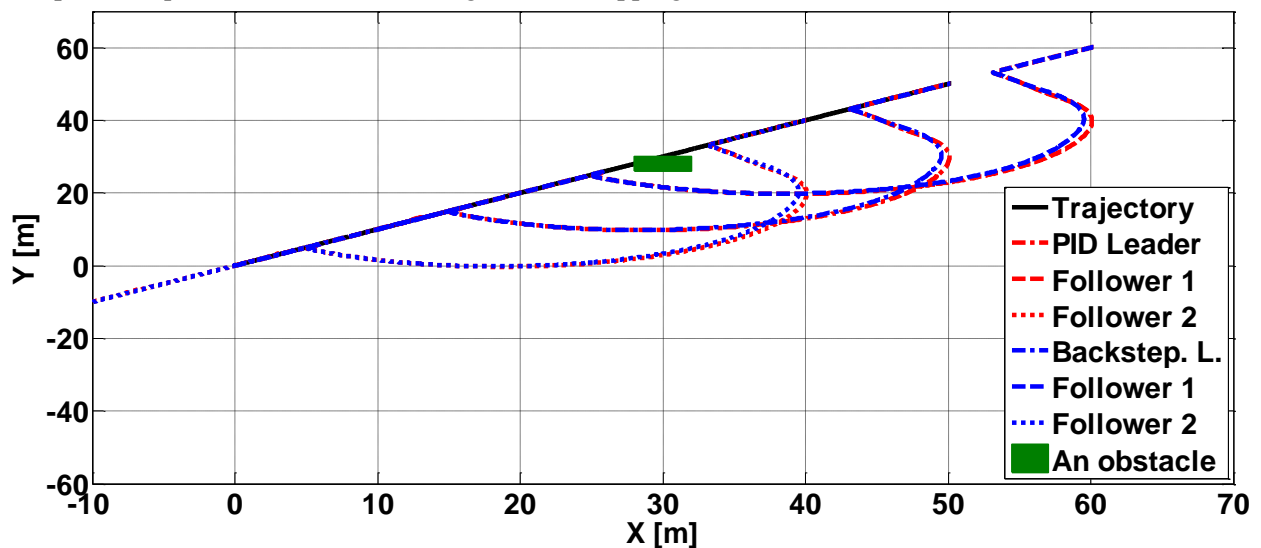
Figure 12. The obstacle avoidance by the cooperative quadrotors controlled by PID and backstepping controllers.

From the simulation results; the proposed controllers succeeded in tracking trajectories in different proposed scenarios keeping the geometric formation reconfiguration of the team of cooperative quadrotors. The resulted performances are sufficient according to PID and the backstepping control synthesis algorithms. Both controllers can stabilize and control the cooperative quadrotors in obstacle-free and obstacle-laden surroundings.

4.3. *Noise attenuation and wind disturbance rejection:*

To check the impact of noise, the altitude sensor is considered to be affected by a white Gaussian noise Figure 13 shows the trajectory tracking of the cooperative quadrotors controlled by PID and backstepping controllers in *Z*-orientation in presence of measurement noise affected the altitude sensor and compares between the obtained results. The results show that the noise attenuation of the cooperative quadrotors controlled using the backstepping controller is better than that obtained using the PID controller.
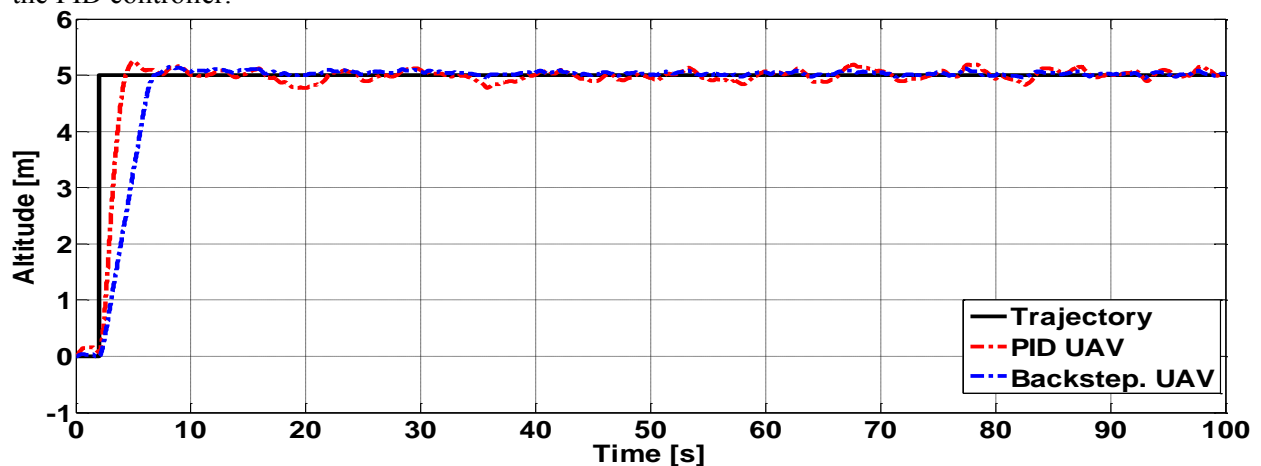
Figure 13. The noise attenuation of the cooperative quadrotors controlled by PID and backstepping controller in *Z*-orientation when the altitude sensor is affected by noise.

To study disturbance rejection of both controllers, wind disturbance is considered to affect the cooperative quadrotors in two opposite directions every 10 seconds with a wind duration effect for 2 seconds. Figure 14 shows the trajectory tracking of the cooperative quadrotors controlled by PID and backstepping controllers in *Z*-orientation in presence of wind disturbance and compares between the obtained results. The results show that the wind disturbance rejection of cooperative quadrotors controlled using the backstepping controller is better than that obtained using the PID controller.
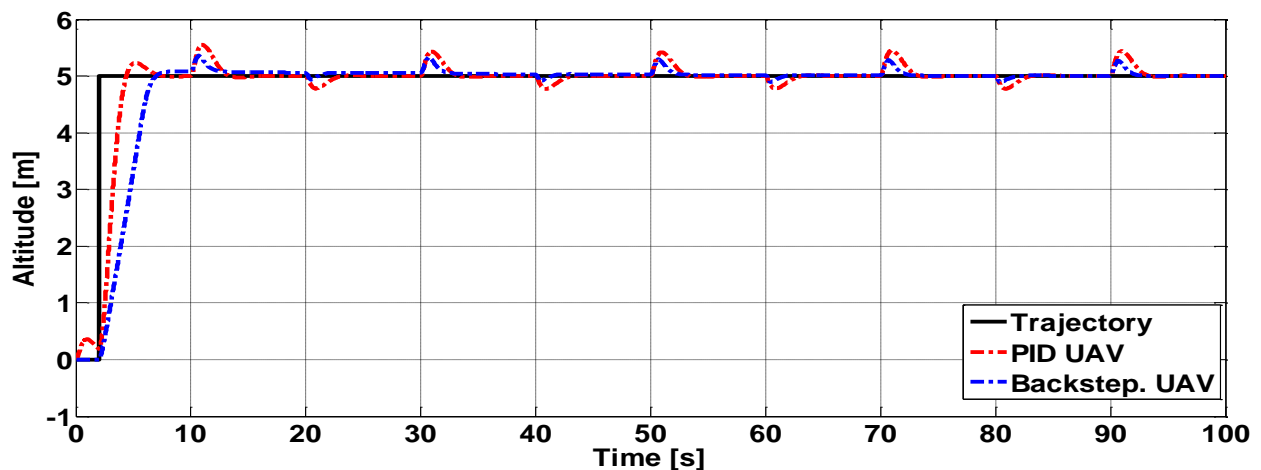
Figure 14. The trajectory tracking of the cooperative quadrotors controlled by PID and backstepping controllers in *Z*-orientation under the effect of wind disturbance.

5. Conclusion

In this paper, PID and backstepping controllers are developed for resolving the formation reconfiguration problem for a team of cooperative quadrotors. A complete mathematical model for the quadrotor under study is introduced. Moreover, a relation between thrust force and RPM is proved experimentally. A collision avoidance algorithm is introduced where the team of cooperative UAV reconfigures its formation in a manner that ensures the safety of the entire team members. The simulation results display a successful steady flight achieved for both controllers in the absence of external noise and disturbance for obstacle-free and obstacle-laden surroundings. The cooperative UAV team succeeded to track the desired path respecting the velocity and separating span constraints. The noise attenuation for both controllers is considered when the altitude sensor is affected by white Gaussian noise. The results show that the backstepping controller is better than the PID controller for noise attenuation. When dealing with wind disturbance, the backstepping controller shows better disturbance rejection than the PID controller.

References

[1]   F. S. C. Ito*, et al.*, "Cooperative UAV formation control simulated in X-plane," in *Unmanned Aircraft Systems (ICUAS), 2017 International Conference on*, 2017, pp. 1522-1529.

[2]   H. Zhang*, et al.*, "Three-dimensional optimal formation reconfiguration for Multi-UAVs based on Chebyshev pseudospectral method," in *Guidance, Navigation and Control Conference (CGNCC), 2016 IEEE Chinese*, 2016, pp. 1253-1258.

[3]   X. Li*, et al.*, "Formation reconfiguration based on distributed cooperative coevolutionary for multi-UAV," in *Intelligent Control and Automation (WCICA), 2016 12th World Congress on*, 2016, pp. 2308-2311.

[4]   A. Sarhan and M. Ashry, "Self-Tuned PID Controller for the Aerosonde UAV Autopilot," *International Journal of Engineering Research & Technology (IJERT),* vol. 2, pp. 2278-0181, 2013.

[5]   E. N. Mobarez*, et al.*, "Comparative robustness study of multivariable controller of fixed wing Ultrastick25-e UAV," in *2018 14th International Computer Engineering Conference (ICENCO)*, 2018, pp. 146-150.

[6]   M. El-Khatib and W. Hussein, "Design, modelling, implementation, and intelligent fuzzy control of a hovercraft," in *Unmanned Systems Technology XIII*, 2011, p. 80450L.

[7]   A. Desoky*, et al.*, "Modeling and Simulation of a Vision-Based Autonomous Vehicle."

[8]   A. Desoky*, et al.*, "Implementation of Vision-Based Trajectory Control for Autonomous Vehicles."

[9]   S. Norouzi Ghazbi*, et al.*, "QUADROTORS UNMANNED AERIAL VEHICLES: A REVIEW," *International Journal on Smart Sensing & Intelligent Systems,* vol. 9, 2016.

[10]   S. Gupte*, et al.*, "A survey of quadrotor unmanned aerial vehicles," in *Southeastcon, 2012 proceedings of ieee*, 2012, pp. 1-6.

[11]   A. Zulu and S. John, "A review of control algorithms for autonomous quadrotors," *arXiv preprint arXiv:1602.02622,* 2016.

[12]   X. Zhang*, et al.*, "A Survey of Modelling and Identification of Quadrotor Robot," *Abstract and Applied Analysis,* vol. 2014, p. 16, 2014.

[13]   F.-y. Zheng*, et al.*, "Adaptive constraint backstepping fault-tolerant control for small carrier-based unmanned aerial vehicle with uncertain parameters," *Proceedings of the Institution of Mechanical Engineers, Part G: Journal of Aerospace Engineering,* vol. 230, pp. 407-425, 2016.

[14]   M. F. A. Rahman*, et al.*, "Implementation of quadcopter as a teaching tool to enhance engineering courses," in *2016 IEEE 8th International Conference on Engineering Education (ICEED)*, 2016, pp. 32-37.

[15]   L. Li*, et al.*, "Survey of advances in control algorithms of quadrotor unmanned aerial vehicle," in *Communication Technology (ICCT), 2015 IEEE 16th International Conference on*, 2015, pp. 107-111.

[16]   Y. Li and S. Song, "A survey of control algorithms for quadrotor unmanned helicopter," in *Advanced Computational Intelligence (ICACI), 2012 IEEE Fifth International Conference on*, 2012, pp. 365-369.

[17]   K. A. Ghamry*, et al.*, "Real-time autonomous take-off, tracking and landing of UAV on a moving UGV platform," in *2016 24th Mediterranean Conference on Control and Automation (MED)*, 2016, pp. 1236-1241.

[18]   M. A. Kamel*, et al.*, "Fault-tolerant cooperative control design of multiple wheeled mobile robots," *IEEE Transactions on control systems technology,* vol. 26, pp. 756-764, 2018.

[19]   H. Zhang*, et al.*, "Time-optimal control for formation reconfiguration of multiple unmanned aerial vehicles," in *Control Conference (CCC), 2016 35th Chinese*, 2016, pp. 5630-5635.

[20]   A. T. Hafez*, et al.*, "Solving multi-UAV dynamic encirclement via model predictive control," *IEEE Transactions on control systems technology,* vol. 23, pp. 2251-2265, 2015.

[21]   A. Hafez and S. Givigi, "Formation reconfiguration of cooperative UAVs via Learning Based Model Predictive Control in an obstacle-loaded environment," in *Systems Conference (SysCon), 2016 Annual IEEE*, 2016, pp. 1-8.

[22]   A. T. Hafez*, et al.*, "Cooperative unmanned aerial vehicles formation via decentralized lbmpc," in *2015 23rd Mediterranean Conference on Control and Automation (MED)*, 2015, pp. 377-383.

[23]   A. T. Hafez*, et al.*, "Multiple cooperative uavs target tracking using learning based model predictive control," in *2015 International Conference on Unmanned Aircraft Systems (ICUAS)*, 2015, pp. 1017-1024.

[24]   M. A. Kamel*, et al.*, "Design of fault-tolerant cooperative control algorithm applied to WMRs against actuator faults," in *2016 American Control Conference (ACC)*, 2016, pp. 7092-7097.

[25]   M. A. Kamel*, et al.*, "Real-time fault-tolerant cooperative control of multiple UAVs-UGVs in the presence of actuator faults," *Journal of Intelligent & Robotic Systems,* vol. 88, pp. 469-480, 2017.

[26]   U. Abou-Zayed*, et al.*, "Implementation of Local Optimal Controller based on model identification of multi-mass electromechanical servo system," in *Proceedings of the 27th IASTED International Conference on Modelling, Identification, and Control*, 2008.

[27]   U. Abou-Zayed*, et al.*, "Experimental Open-loop and Closed-loop Identification of a Multi-mass Electromechanical Servo System," in *ICINCO-SPSMC*, 2008, pp. 188-193.

[28]   S. Bouabdallah*, et al.*, "Design and control of an indoor micro quadrotor," in *Robotics and Automation, 2004. Proceedings. ICRA'04. 2004 IEEE International Conference on*, pp. 4393-4398.

[29]   S. Bouabdallah*, et al.*, "PID vs LQ control techniques applied to an indoor micro quadrotor," in *Proc. of The IEEE International Conference on Intelligent Robots and Systems (IROS)*, 2004, pp. 2451-2456.

[30]   M. Mahfouz and S. A. Kader, "Quadrotor unmanned aerial vehicle controller design and synthesis," in *Computer Engineering & Systems (ICCES), 2015 Tenth International Conference on*, 2015, pp. 60-66.

[31]   A. Oda*, et al.*, "Robust clos guidance and control part-1: System modeling and uncertainty evaluation," in *14th International Conference on Aerospace Sciences & Aviation Technology*, 2010.

[32]   M. Elbaioumy*, et al.*, "Modelling and Simulation of Surface to Surface Missile General Platform," *Advances in Military Technology,* vol. 13, 2018.

[33]   M. Mahfouz, "Neuro Fuzzy Adaptive Control and its Application to Unmanned Air Vehicle [MSc. thesis]," Military Technical College in Cairo, Egypt, 2015.

[34] M. Mahfouz, *et al.*, "Design and control of quad-rotor helicopters based on adaptive neuro-fuzzy inference system," *International Journal of Engineering Research Technology (IJERT),* vol. 2, pp. 479-485, 2013.

[35] R. M. Murray, *et al.*, *A mathematical introduction to robotic manipulation*: CRC press, 1994.

[36] J. G. Leishman, *Principles of helicopter aerodynamics*: Cambridge University Press, 2006.

[37] G. Fay, "Derivation of the aerodynamic forces for the mesicopter simulation," ed, 2001.

[38] K. P. Valavanis, *Advances in Unmanned Aerial Vehicles: State of the Art and the Road to Autonomy*: Springer, 2008.

[39] S. Bouabdallah and R. Siegwart, "Full control of a quadrotor," in *Intelligent robots and systems, 2007. IROS 2007. IEEE/RSJ international conference on*, 2007, pp. 153-158.

[40] M. Wierema, "Design, implementation and flight test of indoor navigation and control system for a quadrotor UAV," *Master of Science in Aerospace Engineering at Delft University of Technology,* 2008.

[41] M. Mahfouz, *et al.*, "Formation Configuration for Cooperative Multiple UAV Via Backstepping PID Controller," in *2018 AIAA SPACE and Astronautics Forum and Exposition*, ed: American Institute of Aeronautics and Astronautics, 2018.

[42] A. Azzam and X. Wang, "Quad rotor arial robot dynamic modeling and configuration stabilization," in *Informatics in Control, Automation and Robotics (CAR), 2010 2nd International Asia Conference on*, 2010, pp. 438-444.

[43] J. Basilio and S. Matos, "Design of PI and PID controllers with transient performance specification," *IEEE Transactions on education,* vol. 45, pp. 364-370, 2002.

[44] A. Habashi, *et al.*, "Comparative Study Among Different Control Techniques For Stabilized Platform," *Engineering Science and Military Technologies,* vol. 2, 2018.

[45] A. Habashi, *et al.*, "Controller Design for Line of Sight Stabilization System," *International Journal of Engineering Research and Technology,* 2015.

[46] H. Hendy, *et al.*, "Controller parameters tuning based on transfer matrix method for multibody systems," *Advances in Mechanical Engineering,* vol. 6, p. 957684, 2014.

[47] C.-C. Yu, *Autotuning of PID controllers: A relay feedback approach*: Springer Science & Business Media, 2006.

[48] J. Connor, *et al.*, "Using particle swarm optimization for PID optimization for altitude control on a quadrotor," in *Universities Power Engineering Conference (AUPEC), 2017 Australasian*, 2017, pp. 1-6.

[49] K. J. Åström and T. Hägglund, *PID controllers: theory, design, and tuning* vol. 2: Instrument society of America Research Triangle Park, NC, 1995.

[50] D. P. Raymer, *Aircraft design: a conceptual approach*: American Institute of Aeronautics and Astronautics Reston, 2006.

[51] M. Ashry, *et al.*, "Comparative robustness study of multivariable controllers for a gas turbine engine," in *IASTED International Conference on Modelling, Identification, and Control*, 2008.

[52] M. M. Ashry, *et al.*, "Tuning of digital PID controller parameters using local optimal control," in *2008 16th Mediterranean Conference on Control and Automation*, 2008, pp. 587-592.

[53] M. Ashry, *et al.*, "Control of multivariable systems using modified local optimal controller," *IFAC Proceedings Volumes,* vol. 41, pp. 8767-8772, 2008.

[54] A. Onsy, *et al.*, "Effect of Slow-Active Suspension Controller Design on the Performance of Anti-Lock Brake System," in *15 th International Conference on ASAT-15, Military Technical College, Kobry Elkobbah, Cairo, Egypt*, 2013.

[55] M. A. Elkhayat, *et al.*, "Backstepping control using Single Gimbal Control Moment Gyro with parameter uncertainties," in *2016 IEEE Aerospace Conference*, 2016, pp. 1-9.

[56] I. Mahjri, *et al.*, "A review on collision avoidance systems for unmanned aerial vehicles," in *International Workshop on Communication Technologies for Vehicles*, 2015, pp. 203-214.